AEROACOUSTICS OF ADVANCED PROPELLERS

John F. Groeneweg
National Aeronautics and Space Administration
Lewis Research Center
Cleveland, Ohio 44135

Abstract

The aeroacoustics of advanced, high-speed propellers (propfans) are reviewed from the perspective of NASA research conducted in support of the Advanced Turboprop Program. Aerodynamic and acoustic components of prediction methods for near and far field noise are summarized for both single and counterrotation propellers in uninstalled and installed configurations. Experimental results from tests at both takeoff/approach and cruise conditions are reviewed with emphasis on: (1) single and counterrotation model tests in the NASA Lewis 9 by 15 (low-speed) and 8 by 6 (high-speed) wind tunnels, and (2) full-scale flight tests of a 9-ft (2.74-m) diameter single rotation wing mounted tractor and a 11.7-ft (3.57-m) diameter counterrotation aft mounted pusher propeller. Comparisons of model data projected to flight with full-scale flight data show good agreement validating the scale model wind tunnel approach. Likewise, comparisons of measured and predicted noise levels show excellent agreement for both single and counterrotation propellers. Progress in describing angle of attack and installation effects is also summarized. Finally, the aeroacoustic issues associated with ducted propellers (very high bypass fans) are discussed.

Introduction

Advanced propeller aeroacoustics research has been a major component of the NASA Advanced Turboprop Program. While energy efficiency was the prime objective, airport community and aircraft cabin noise constraints and structural integrity were essential ingredients determining the content of the overall research effort.[1-3] This paper highlights aeroacoustic results from more than a decade of work. The emphasis is on advanced propeller source noise prediction and measurement in both the low speed takeoff/approach and high-speed cruise regimes which address community and cabin noise, respectively. The results described are the products of NASA Lewis in-house and sponsored research. Both model and full-scale data are compared to predictions based on aerodynamic inputs to acoustic radiation analyses.

The term "advanced propeller" as used here refers to a configuration of the type shown in Fig. 1. The distinguishing features of this class of propeller (or propfan) are very thin swept blades, typically 8 to 12 in number, designed for cruise Mach numbers of the order of 0.8. The particular propeller shown undergoing static tests in Fig. 1 is a 9-ft (2.74-m) diameter, wing-mounted tractor configuration[4] which has eight blades and a design tip speed of 800 ft/sec (244 m/sec). Helical tip Mach number at cruise is supersonic (e.g., M = 1.15).

Figure 2 is a flow chart outlining the aerodynamic and acoustic elements involved in analyzing advanced propeller noise generation. Flow field and configuration complexity increases as we move from left to right in the three column headings. Beginning on the left, for a single rotation propeller in a uniform flow the steady loading and thickness noise sources defined by the steady blade pressures and the blade geometry, respectively, feed into a source noise radiation model whose output is the near and far field noise. It should be noted that this discussion pertains to tone noise generation since this spectral component dominates the propeller noise spectrum. The second column deals with counterrotation propellers operating in a uniform flow field. This situation requires the description of the additional loading mechanism associated with blade row unsteady aerodynamic interactions produced by blade wakes, vortices and potential flow nonuniformities from one blade row interacting with the other blade row. The unsteady aerodynamic response in the form of fluctuating blade pressures must be input to the source noise radiation model in addition to the steady components for each blade row. Finally, the third column addresses the added complexity of single or counterrotation propellers operating at angle-of-attack or in nonuniform flow fields produced by such things as engine support struts and airframe flow fields.

The discussion in this paper proceeds as follows. Prediction methods for single and counterrotation configurations are reviewed for both steady and unsteady sources. Next, results of model scale experiments are described followed by full-scale flight data from the single rotation Propeller Test Assessment (PTA)[5] and the counterrotation Unducted Fan (UDF)[6] tests. Comparisons of predictions with the data, both model and full scale, are included. Finally, the aeroacoustic issues associated with ducted propeller (very high bypass) configurations are discussed.

Aeroacoustic Prediction Methods

Table I lists various combinations of aerodynamic and acoustic analysis methods which have been addressed in developing computer programs (codes) to deal with the hierarchy of propeller noise generation mechanisms discussed in connection with Fig. 2. The starting points for acoustic predictions are methods to calculate both steady and unsteady propeller flow fields as indicated by the column labeled "aerodynamic input". Acoustic models may apply to single or counterrotation configurations which are either uninstalled or installed, i.e., allow for nonuniform inflow. An indication of the status of the combination of aerodynamic and acoustic analysis codes is indicated following each entry. Overall, the state-of-the-art for aerodynamic predictions has advanced to operational three-dimensional steady and unsteady Euler codes, with active development of three-dimensional steady Navier-Stokes codes underway.

The acoustic radiation models are, with a few exceptions, linear and of two types: time domain[7] or frequency domain.[8] In the steady loading regime lifting line, lifting surface and Euler solutions have been input to either of the two acoustic formulations (items A to C in Table I, Refs. 9-11). For the one case in Table I where nonlinear acoustic propagation comes into play (item C2, Ref. 12), a three-dimensional Euler code is used to directly compute near field pressures with the intention of coupling the results to a linear far field propagation model. Numerical dissipation associated with the computational grid must be carefully considered and much work remains to be done to refine this approach.

Item B in Table I is a unified aerodynamic and acoustic approach developed by Hamilton Standard[8] under a NASA Lewis contract. A three-dimensional linear lifting surface theory is used with some nonlinear aerodynamic modifications to handle induction and leading edge vortex formation at off-design conditions. The single rotation code, which has subroutines to calculate boundary layer refraction and wing shielding, is being evaluated at Hamilton Standard and NASA Lewis. Navier-Stokes input to acoustics models awaits the refinement of the application of viscous flow solvers to advanced propeller configurations.

In the unsteady regime dealing with counterrotation and installation effects, considerable progress has been made using linear unsteady aerodynamic response models. The three approaches labeled E1 to E3 have been developed by General Electric[13,14] under NASA Lewis contracts. The uninstalled counterrotation code uses a mix of aerodynamic methods: section lift and drag determined by separate means are input as a function of radius for each rotor along with a choice of chordwise loading distribution. A semi-empirical, wake-vortex model gives gust input to the downstream blade row whose unsteady loading is given by a linear response function. Unequal rotor speeds and blade numbers are handled by the analysis. Installed single and counterrotation codes (E2 and E3) use an actuator disk and either quasi-steady or linear lift response to calculate unsteady loading contributions to the noise for operation at angle-of-attack or in nonuniform flow. An additional modification to the steady loading and thickness contributions has been incorporated to account for the steady flow component in the propeller plane for angle-of-attack situations.[15] The cross-disk component has the effect of changing the radiation efficiency of the acoustic modes radiating from the propeller.

Linear unsteady aerodynamic response has been included in the unsteady lifting surface theory for single rotation and has also been incorporated into a counterrotation analysis (item F). Viscous wakes and leading edge vortices are modelled semi-empirically. Fully three-dimensional unsteady Euler equation solutions have recently been obtained for the case of a propeller at angle-of-attack (item G, Ref. 16) and acoustic calculations are in progress. During one revolution of the propeller, individual blade loading is computed to vary by a factor of more than eight. Unsteady Navier-Stokes solutions (item H) remain to be developed following the validation of steady viscous codes now underway.

Experimental Results and Comparisons with Predictions

The data reported here are primarily from four sources: the model scale tests in the NASA Lewis 8- by 6-ft and 9- by 15-ft wind tunnels, and the full-scale flight tests of the PTA, and 727/UDF aircraft which included formation flights by the instrumented Lewis Learjet. Advanced propeller acoustic data also exist from the United Technologies Acoustic Research Tunnel, the General Electric Cell 41 facility, and the Boeing Transonic Wind Tunnel.[17,18] In addition, flight data were acquired on the 727/UDF,[19] the MD-80/UDF[20] and the MD-80/578 DX.[21]

Wind Tunnel Aeroacoustic Measurements

Extensive near field model data in the cruise regime were obtained in the Lewis 8- by 6-ft wind tunnel by measuring with an array of transducers which are flush mounted in a metal plate as shown in Fig. 3. This technique tends to minimize the effects of any reflections from the porous walls in comparison to a freestream microphone measurement, and the refraction by the boundary layer on the plate is less than for a microphone mounted in the tunnel wall where the boundary layer is much thicker. A large body of single and counterrotation data has been acquired using the technique. Acoustic measurements at high-speed cruise conditions up to 0.9 Mach number are particularly difficult upstream of the propeller source due to boundary layer refraction at any surface exposed to the flow. In the case of the flush mounted transducer approach described above, refraction of upstream propagating sound causes erroneously low levels to be measured as the boundary layer thickness or the sound frequency is increased. On the other hand, attempts to design wall acoustic treatment to achieve anechoic tunnel conditions at high subsonic Mach numbers are greatly complicated by refraction at upstream locations. A comparison of results from the Lewis 8- by 6-ft wind tunnel with those performed on the same propeller model in the acoustically treated Boeing Transonic Wind Tunnel are shown in Fig. 4.[22] Agreement is generally quite good aft of the plane of rotation. At the higher harmonics the effect of refraction at forward angles on the plate in the 8- by 6-ft tunnel is evident. Attempts to correct the data using a boundary layer refraction model were unsuccessful at far forward angles indicating the need for a more refined refraction analysis.[23] Figure 5 compares full-scale flight data obtained on the fuselage and boom of the PTA aircraft with the 9-ft (2.74-m) diameter SR-7L propeller to the scaled 8- by 6-ft tunnel data obtained on the 2-ft (0.61-m) diameter model of the SR-7. Agreement is quite good for this flight condition where the angle-of-attack into the propeller was nearly zero corresponding to the zero angle-of-attack of the wind tunnel model.

Model data at low speed conditions representative of takeoff/approach were obtained in the Lewis 9- by 15-ft Anechoic Wind Tunnel shown in Fig. 6. A counterrotation propeller model is shown along with a traversing sideline microphone and a polar microphone probe installed on the model itself. The walls of the tunnel are acoustically treated with a 13-in. (33-cm) thick double layer bulk absorber treatment designed to be

anechoic down to 250 Hz.[24] Model tone frequencies were typically 500 Hz and above. Comparisons of the data taken on the same model propeller in an anechoic free jet facility showed agreement generally within 2 dB.[14] In the 9- by 15-ft tunnel installation the model may be rotated in the horizontal plane to obtain acoustic data over a wide range of propeller axis angles-of-attack.

Single Rotation Model Acoustic Results

Single rotation tone data have been obtained at cruise conditions over a range of helical tip Mach numbers at constant advance ratio for three blade pitch angles as shown in Fig. 7.[25] The maximum fundamental tone levels increase until helical tip Mach number reaches about 1.1. At higher supersonic Mach numbers tone levels show a varied behavior depending on the blade loading (pitch). None of the theories for single rotation noise discussed in connection with Table I predict these tone variations at high Mach numbers (e.g., the predictions for the similar SR-3 propeller, Ref. 13). At high Mach numbers, thickness noise tends to dominate in the theories in contrast to the data which shows substantial loading dependence. It should be noted that thrust or efficiency is not falling off[25] so that deterioration in propeller performance is not an explanation for the phenomena. This long-standing data-theory discrepancy at supersonic helical tip Mach numbers remains one of the unsolved problems of advanced propeller acoustics.

At low speed takeoff/approach conditions, the propeller is operating far from the aerodynamic design point. When the takeoff noise was predicted over a range of blade loadings, the fundamental tone level was underpredicted to an increasing degree as loading was increased as shown in Fig. 8.[26] This discrepancy is attributable to altered blade loading due to the formation of a leading edge vortex on the suction surface which merges with the tip vortex as determined by flow visualization[27] and computed using a three-dimensional Euler code on a refined grid as illustrated by the particle paths in Fig. 9. This phenomena is handled in a semi-empirical way in the lifting surface aeroacoustic model being developed (item F, Table I).

One of the simplest ways of obtaining unsteady propeller loading is to pitch the propeller axis at an angle to the incoming flow. Results of varying the propeller angle-of-attack for a counterrotation model (F7/A7) at low speed takeoff/approach conditions are shown for the fundamental, rotor-alone tone directivities in Fig. 10.[28] These directivities were measured at an azimuthal position corresponding to an observer directly beneath an aircraft on takeoff or approach. Tones from both rotors behave in a similar manner with significant increases for positive and decreases for negative angles of attack, respectively. The levels change on the order of 3/4 dB per degree of propeller axis pitch. Initial attempts to predict these results were unsuccessful when an unsteady aerodynamic response model for the changing blade loading due to change in incidence with circumferential position was used.[15] As shown in Fig. 11, where azimuthal directivities are plotted for the F7/A7 counterrotation model, the unsteady blade response model (the dashed curve) greatly underpredicted the data. However, when the steady flow component in the plane of the propeller was accounted for,[15] the changes in the steady loading and thickness components due to the altered radiation efficiency improved the prediction significantly (the solid curve). Since the phenomena, which is more prominent for high tip speed, heavily loaded propellers with a large number of blades, was calculated only to first order in crossflow Mach number, further improvement may result as the analysis is refined.

Installation effects for single rotation have been explored with a wing-mounted tractor configuration at takeoff/approach conditions using the scale model SR-7 propeller.[29] Angle-of-attack of the wing-prop assembly was varied and the angle between the propeller centerline and the wing chordline was varied in a manner analogous to the nacelle tilt variations in the full-scale PTA flight tests with the SR-7L. The effects of propeller axis droop are summarized in Fig. 12 where maximum tone noise is plotted versus angle-of-attack for four droop angles. It can be seen that droop has little effect at the fundamental and only small influence at the second harmonic. The presence of the wing increases the tone levels a few decibels and also increases the rate of change of tone level with angle-of-attack.

Counterrotation Model Acoustic Results

The distinguishing feature of a counterrotation compared to a single rotation noise spectrum is the appearance of many of the possible sum and difference frequencies of the two rotors in addition to all harmonics of each separate rotor. A sample spectrum at takeoff/approach conditions is shown in Fig. 13 for the F7/A7 propeller with 11 x 9 (forward x aft) blades. As is typically the case, the interaction tones at $nBPF_1 + mBPF_2$ dominate the spectrum at frequencies above the fundamental tones of the two rotors. While the fundamental tones peak near the plane of rotation, the interaction tones tend to peak away from the plane of rotation.

Directly below the aircraft in the plane of rotation of the aft propeller, the fundamental tones, vary strongly with angle of attack as shown in Fig. 14 (compare the levels with Fig. 10). In contrast, the interaction tones at this location are quite insensitive to angle of attack. Of course, the azimuthal directivity is decidedly asymmetric at nonzero angles of attack.

At cruise conditions the rotor alone tones controlled by thickness and loading tend to dominate the tone levels compared to interaction tones, particularly near the plane of rotation. Figure 15 shows the tone directivities measured in the near field of the F1/A1 propeller which was run with 9 x 8 blades producing a spectrum with all tones well separated in frequency.[30] The second harmonics, the first interaction tone and the sum of the three are shown. The interaction tone is more than 10 dB down from the second harmonics in the vicinity of the plane of rotation. Rotor alone fundamental tones are of the order of 10 dB higher than the rotor alone second harmonics. In short, interaction noise at cruise is only a contributor toward the propeller axis. Predictions for this propeller using the theory of

Ref. 14 are shown in Fig. 16 for the second harmonics. Agreement with the 8- by 6-ft wind tunnel data is quite good except at a few forward angles.

One of the aspects of counterrotation takeoff/approach noise studied in the 9- by 15-ft Anechoic Wind Tunnel was the effect of rotor-to-rotor spacing on interaction tones for an equal diameter and a reduced diameter aft rotor, designated F7/A7 and F7/A3, respectively. Measured tone levels for the 11 x 9 configurations are shown in Fig. 17[31] as a function of spacing between the rotor pitch change axes. If rotor-to-rotor interaction noise is strongly influenced by tip flow disturbances from the forward rotor such as vortices in addition to the spanwise viscous wakes, a reduced diameter aft rotor could avoid the vortex interaction. In that case, as spacing is increased, interaction tones would be expected to fall off at a faster rate because viscous wake decay with downstream distance is more rapid than vortex decay. For the data in Fig. 17, F7/A7 and F7/A3 were absorbing the same power at the same rotational speed and produced nearly equal thrust by setting A3 at a higher pitch than A7. As expected, Fig. 17(a) shows that fundamental rotor-alone tones are not influenced by spacing. The first two interaction tones, shown in Fig. 17(b), do decrease more rapidly with spacing and reach lower levels for F7/A3 compared to F7/A7. However, at the closest spacing F7/A3 has higher interaction tone levels possibly associated with potential field interaction of the highly loaded A3 with F7. In fact, diagnostic tests using bladed mounted pressure transducers[32] showed that a transducer on F7 sensed an unsteady pressure at a frequency corresponding to the number of times per second that the aft rotor passed the instrumented forward blade.

When the counterrotation theory[14] was applied to predict levels of the first three interaction tones for F7/A7, the comparisons in Fig. 18 were obtained. The shapes and levels of the measured and predicted directivities are generally in agreement except for the $2BPF_1 + BPF_2$ tone at aft angles. Aerodynamic modelling of the forward rotor wake and tip vortex is influential in determining the strength of each interaction tone which also corresponds to a particular acoustic mode. A range of data-theory comparisons including F7/A3 propeller, showed a tendency to overpredict the benefits of using a reduced diameter aft rotor.[14]

The effects on noise of an aft mount installation including an upstream support pylon and the presence of a body simulating the after portion of an aircraft fuselage have also been investigated at takeoff/approach conditions including angle-of-attack.[33] Additional noise at the rotor alone tones and their harmonics is generated by the pylon wake interacting with the blade rows. The magnitudes of the increases for an observer during flyover are only a few decibels for the fundamentals, but may be 5 dB or more at harmonics. When the model is pitched to angle of attack, the pylon acts as a vane to preswirl the flow into the rotors. The preswirl has the effect of increasing the loading on one row and decreasing it on the other. The acoustic effects for the F7/A3 propeller are shown in Fig. 19 as maximum forward rotor fundamental tone levels versus angle-of-attack at two azimuthal locations corresponding to $\phi = 0°$ directly above and $\phi = 180°$ directly below the propeller. It is seen that the maximum tone levels are increased or decreased at nonzero angle-of-attack depending on azimuthal position and whether the blade angles are adjusted to equalize forward and aft rotor torques in the presence of pylon induced inflow swirl.

As can be seen in Fig. 20, the presence of the pylon and aft fuselage simulation also tends to increase the fundamental tone levels in the azimuthal direction at $\phi = 90°$, i.e., in the horizontal plane though the propeller axis.[34] Reflection from the simulated aft fuselage is probably the controlling factor. In general, data of the type in Figs. 19 and 20 are indicative of the fact that installation effects for counterrotation propellers can be varied and complex.

Full-Scale Flight Results

Two full-scale flight test series were conducted: the PTA tests of the wing-mounted 9-ft (2.74-m) diameter single rotation SR-7L shown in Fig. 21, and the UDF/727 tests of the aft-mounted 11.7-ft (3.57-m) diameter counterrotation F7/A7 shown in Fig. 22. Additional flight tests of counterrotation configurations were conducted on an MD-80 aircraft,[20,21] the detailed acoustic data from which are not available for presentation here.

For near field fundamental tone measurements made at cruise conditions, the favorable comparison between the full-scale PTA flight data and scaled model 8- by 6-ft wind tunnel data was discussed in connection with Fig. 5. Those flight data were taken at a nacelle tilt of -1° and aircraft attitude in flight which produced a small angle of attack of the propeller axis with respect to the flow. The wind tunnel data were taken with axial flow into the model. When the nacelle tilt was varied to +2° and -3°, a pronounced azimuthal asymmetry was observed in the tone directivity as indicated by the fuselage and boom data shown in Fig. 23.[35] Fuselage measurements were made by linear transducer arrays, and boom measurements were made by a linear array at the wing tip 9.4° below the horizontal. Maximum sound pressure levels at blade passage frequency are plotted versus nacelle tilt for four propeller tip speeds. The inflow angle ψ is an estimate of the actual angle of the flow into the propeller relative to the propeller axis. As nacelle tilt is increased, fuselage levels decrease while boom levels increase. The most rapid rates of change occurred at the lower tip speeds where the loading component of the source is stronger relative to the thickness component.

Detailed three-dimensional unsteady Euler calculations[16,36] have been made with the objective of obtaining detailed unsteady blade loadings for input to acoustic radiation codes, the ultimate goal being the prediction of data of the type shown in Fig. 23. Calculated individual instantaneous blade loadings for the three nacelle tilts tested are shown in Fig. 24 for azimuthal locations on the fuselage and boom sides, respectively. Note that the instantaneous loadings at these two locations vary qualitatively in the same manner as the maximum fuselage and boom tone levels. Acoustic calculations using the instantaneous blade

pressures computed throughout one propeller revolution are in progress.

In addition to the comparison of single rotation model data obtained in the Lewis 8- by 6-ft wind tunnel to full-scale PTA data (Fig. 5), counterrotation model data obtained in the same facility have been compared to full-scale UDF flight data. The data were obtained by formation flight of the instrumented Lewis Learjet (shown in Fig. 21 with the PTA aircraft) with the 727 aircraft acting as a flying test bed for the UDF (Fig. 22). Scaled F7/A7 data from the 8- by 6-ft wind tunnel are compared with the flight data in Fig. 25.[19] There is good agreement between the model and full-scale data, particularly since the in-flight automatic pitch control system did not allow the full-scale aft blade pitch angles to be matched with available model data. Predictions of the UDF tones measured by the Learjet at cruise conditions also showed excellent agreement except at the farthest forward angles.[14]

Flyover noise data at simulated community conditions were measured on the ground and are compared to predictions as shown in Fig. 26 from Ref. 14. The flyover directivities are the tone sums at the fundamental, 2BPF and 3BPF, respectively. Note that the tone sums at 2BPF and 3BPF include rotor-alone plus interaction tones. Flight conditions were an aircraft Mach number of 0.255, engine pressure ratio of 3.05, pressure altitude of 4340 ft (1323 m), and forward and aft rotor rpm's of 1357 and 1293, respectively. The curves labeled "uninstalled" are the output of the isolated counterrotation model, and the "installed" curves are predictions for installation effects on the rotor alone harmonics only. Except for the tendency to underpredict the fundamental tone sum in the forward arc even when installation effects are included in the prediction, the overall agreement between measured and predicted levels is very good. Of course inclusion of installation effects for the higher rotor alone harmonics (Figs. 26(b) and (c)) has negligible effect on the totals predicted because those sums are controlled by rotor-rotor interaction tones.

Ducted Propellers

Large, long range aircraft typically have engines of large thrust size mounted under the wing. Unducted rotors, even in counterrotation configurations of the required thrust size, are too large in diameter for this type of installation. Thus interest is currently focusing on ducted propellers (very high bypass fans). Figure 27 lists some of the technical issues for these configurations with the upper half of the figure addressing high-speed cruise and the lower half addressing low-speed takeoff/approach operation. The discussion here will focus and elaborate on the aeroacoustic aspects. At cruise where the acoustic concern is achieving acceptable cabin noise levels, a duct offers some fuselage shielding in the plane of the propeller. However, the cowl must be very thin and short to minimize cruise drag which decreases shielding and leaves little space or depth for acoustic treatment. Large diameter rotors will tend to run at lower tip speeds and have fewer blades than current turbofans. These factors push the tones to lower frequencies which require deeper treatments and may move higher harmonics into the frequency range for high annoyance.

At low flight speeds typical of takeoff/approach operations, far field noise is the issue. Inlet distortions associated with high angles of attack, rotor-stator and rotor-strut interactions are potential sources of additional noise. The problem of rotor operation in flow nonuniformities produced by the cowl support struts, even if integrated in the stator vanes, is aggravated by the added structural requirements associated with holding small rotor tip clearances with larger engine diameters and shorter, thinner cowls. Vane-blade ratios chosen for tone cutoff must be reevaluated to confirm cutoff effectiveness for short ducts. The comments about acoustic treatment lengths and depths, and the spectral changes mentioned for the cruise regime apply to the takeoff/approach regime as well.

A first attempt at estimating the acoustic shielding associated with the short duct was made using a simple barrier model of the cowl[37] for a range of cowl lengths and placements of the rotor source within a given length cowl. Figure 28 shows attenuations due to duct shielding for duct lengths ranging from 0.25 to 1.0D (D = rotor diameter for the case where the rotor was located one-third of the duct length from the inlet. The results are for the fundamental tone having a wavelength equal to D/2. Attenuations are plotted versus fore and aft sideline position, x/D, at a sideline distance equal to 0.8D from the rotor tip. Of course, as the duct is shortened peak attenuation drops from nearly 17 to 7 dB. Higher harmonics or a higher fundamental frequency would experience more attenuation. Calculations with refined models are needed for actual acoustic modes and cowl geometries.

Concluding Remarks

Considerable progress has been made in understanding the aeroacoustics of advanced propellers over the past decade that NASA has researched the subject in conjunction with the Advanced Turboprop Project. On the prediction side, three-dimensional steady and unsteady aerodynamics codes are available to provide input to acoustic radiation models which account for thickness and loading noise components. A large body of propeller acoustic data is available from both model and full-scale experiments spanning the range of operation from low-speed takeoff/approach to high-speed cruise. When the model wind tunnel data are projected to full-scale flight, the comparisons are very encouraging. Similarly, when the predictions using the analytical tools are compared with data, agreement is often remarkably good. While progress has been made in handling angle of attack, refinement of the theory is needed to describe the azimuthal directivity more accurately. Work remains to be done on realistic installation geometries and the noise produced by propeller operation in the accompanying complex nonuniform flow fields. Interest is now focusing on ducted propellers (very high bypass fans) because of the installation requirements for large thrust under-the-wing propulsion systems for long range aircraft. These large diameter rotors in short ducts involve a new range of aeroacoustic considerations requiring synthesis and extension of turboprop and turbofan acoustic technology.

REFERENCES

1. Whitlow, J.B., Jr.; and Sievers, G.K.: Fuel Savings Potential of the NASA Advanced Turboprop Program. NASA TM-83736, 1984.

2. Whitlow, J.B., Jr.; and Sievers, G.K.: NASA Advanced Turboprop Research and Concept Validation Program. NASA TM-100891, 1988.

3. Groeneweg, J.F.; and Bober, L.J.: NASA Advanced Propeller Research. NASA TM-101361, 1988.

4. DeGeorge, C.L.: Large Scale Advanced Prop-Fan (LAP). NASA CR-182112, 1988.

5. Little, B.H., et al.: Propfan Test Assessment (PTA). NASA CR-185138, 1989.

6. Reid, C.R.: Overview of Flight Testing of GE Aircraft Engines' UDF Engine. AIAA Paper 88-3082, July 1988.

7. Farassat, F.: Prediction of Advanced Propeller Noise in the Time Domain. AIAA J., vol. 24, no. 4, Apr. 1986, pp. 578-584.

8. Hanson, D.B.: Compressible Helicoidal Surface Theory for Propeller Aerodynamics and Noise. AIAA J., vol. 21, no. 6, June 1983, pp. 881-889.

9. Nystrom, P.A.; and Farassat, F.: A Numerical Technique for Calculation of the Noise of High-Speed Propellers with Advanced Blade Geometry. NASA TP-1662, 1980.

10. Clark, B.J.; and Scott, J.R.: Coupled Aerodynamic and Acoustical Predictions for Turboprops. NASA TM-87094, 1986.

11. Nallasamy, M.; Clark, B.J.; and Groeneweg, J.F.: High-Speed Propeller Noise Predictions: Effects of Boundary Conditions Used in Blade Loading Calculations. J. Aircraft, vol. 25, no. 2, Feb. 1988, pp. 154-162.

12. Korkan, K.D.; von Lavante, E.; and Bober, L.J.: Numerical Evaluation of Propeller Noise Including NonLinear Effects. AIAA J., vol. 24, no. 6, June 1986, pp. 1043-1045.

13. Whitfield, C.E., et al.: High Speed Turboprop Aeroacoustic Study (Single Rotation). Vol. I: Model Development. NASA CR-182257-VOL-1, 1989.

14. Whitfield, C.E.; Mani, R.; and Gliebe, P.R.: High Speed Turboprop Aeroacoustic Study (Counterrotation). Vol. I: Model Development. NASA CR-185241, 1990.

15. Mani, R.: The Radiation of Sound from a Propeller at Angle of Attack. NASA CR-4264, 1990.

16. Nallasamy, M.; and Groeneweg, J.F.: Prediction of Unsteady Blade Surface Pressures on an Advanced Propeller at an Angle of Attack. AIAA 89-1060, Apr. 1989 (Also, NASA TM-102374).

17. Magliozzi, B.: Noise Characteristics of a Model Counter-Rotating Prop-Fans. AIAA Paper 87-2656, Oct. 1987.

18. Janardan, B.A.; and Gliebe, P.R.: Acoustic Characteristics of Counterrotating Unducted Fans from Model Scale Tests. J. Aircraft, vol. 27, no. 3, Mar. 1990, pp. 268-275.

19. Woodward, R.P.; Loeffler, I.J.; and Dittmar, J.H.: Measured Far-Field Flight Noise of a Counterrotation Turboprop at Cruise Conditions. NASA TM-101383, Jan. 1989.

20. Donelson, J.E.; Lewerenz, W.T.; and Durbin, R.T.: UHB Demonstrator Flight Test Program, Phase 2. AIAA Paper 89-2582, July 1989.

21. Chapman, D.C.; Fleury, R.E.; and Smith, D.E.: Testing of the 578-DX Propfan Propulsion System. AIAA Paper 89-2581, July 1989.

22. Dittmar, J.H.: Comparison of Propeller Cruise Noise Data Taken in the NASA Lewis 8- by 6-Foot Wind Tunnel with Other Tunnel and Flight Data. AIAA Paper 89-1059, Apr. 1989. (Also, NASA TM-101976).

23. Dittmar, J.H.; and Krejsa, E.A.: Predicted and Measured Boundary Layer Refraction for Advanced Turboprop Propeller Noise. NASA TM-102365, 1990.

24. Dahl, M.D.; and Woodward, R.P.: Comparison Between Design and Installed Acoustic Characteristics of NASA Lewis 9- by 15-Foot Low-Speed Wind Tunnel Acoustic Treatment. NASA TP-2996, 1990.

25. Dittmar, J.H.; and Stang, D.B.: Cruise Noise of the 2/9 Scale Model SR-7A Propeller. J. Aircraft, vol. 8, no. 8, Aug. 1988, pp. 740-746.

26. Nallasamy, M.; Woodward, R.P.; and Groeneweg, J.F.: High-Speed Propeller Performance and Noise Predictions at Takeoff/Landing Conditions. J. Aircraft, vol. 26, no. 6, June 1989, pp. 563-569.

27. Vaczy, C.M.; and McCormick, D.C.: A Study of the Leading Edge Vortex and Tip Vortex on Prop-Fan Blades. J. Turbomachinery, vol. 109, no. 3, July 1987, pp. 325-331.

28. Woodward, R.P.: Noise of a Model High Speed Counterrotation Propeller at Simulated Takeoff/Approach Conditions (F7/A7). AIAA Paper 87-2657, Oct. 1987 (NASA TM-100206).

29. Woodward, R.P.: Measured Noise of a Scale Model High Speed/Propeller at Simulated Takeoff/Approach Conditions. AIAA Paper 87-0526, Jan. 1987. (Also, NASA TM-88920).

30. Dittmar, J.H.; and Stang, D.B.: Noise Reduction for Model Counterrotation Propeller at Cruise by Reducing Aft-Propeller Diameter. NASA TM-88936, 1987.

31. Woodward, R.P.; and Gordon, E.B.: Noise of a Model Counterrotation Propeller with Reduced Aft Rotor Diameter at Simulated Takeoff/ Approach Conditions (F7/A3). AIAA Paper 88-0263, Jan. 1988. (NASA TM-100254).

32. Heidelberg, L.J.; and Woodward, R.P.: Unsteady Blade Pressure Measurements on a Model Counterrotation Propeller. AIAA Paper 89-1144, Apr. 1989 (Also, NASA TM-102002).

33. Woodward, R.P.: Noise of a Simulated Installed Model Counterrotation Propeller at Angle-of-Attack and Takeoff/Approach Conditions. AIAA Paper 90-0283, Jan. 1990 (Also, NASA TM-102440).

34. Woodward, R.P.; and Hughes, C.E.: Noise of a Model Counterrotation Propeller with Simulated Fuselage and Support Pylon at Takeoff/ Approach Conditions. AIAA Paper 89-1143, Apr. 1989 (Also, NASA TM-101996).

35. Little, B.H.; et. al.: Propfan Test Assessment (PTA): Flight Test Report. NASA CR-182278, 1989.

36. Nallasamy, M.; and Groeneweg, J.F.: Unsteady Euler Analysis of the Flow Field of a Propfan at an Angle of Attack. AIAA Paper 90-0339, Jan. 1990.

37. Dittmar, J.H.: An Estimate of the Noise Shielding on the Fuselage Resulting from Installing a Short Duct Around an Advanced Propeller. NASA TM-100262, 1988.

FIGURE 1. - FULL SCALE ADVANCED PROPELLER ON STATIC TEST STAND.

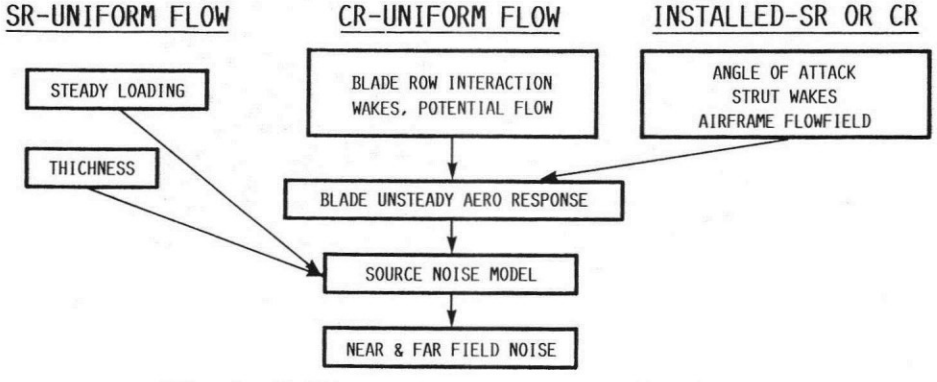

FIGURE 2. - ELEMENTS OF ADVANCED PROPELLER NOISE GENERATION.

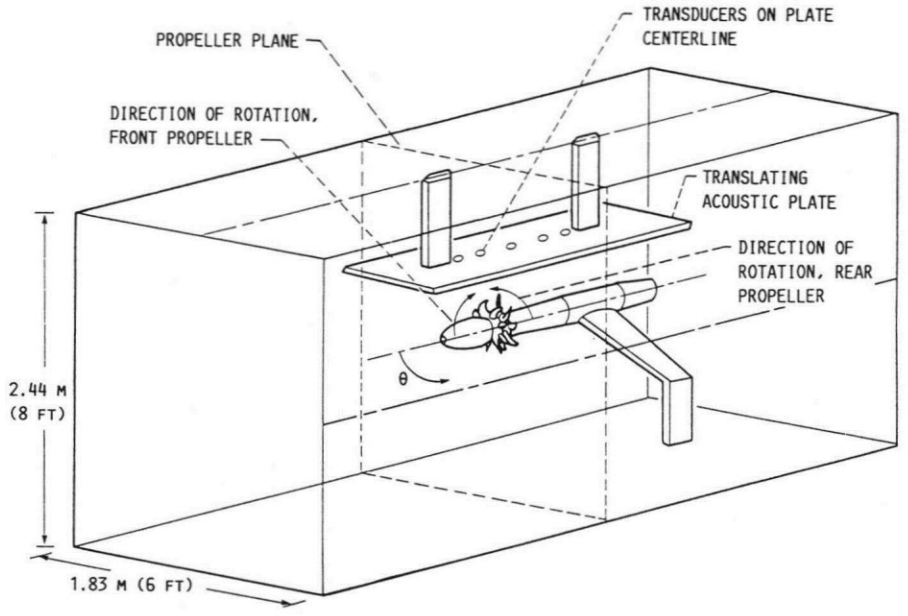

(a) PERSPECTIVE.

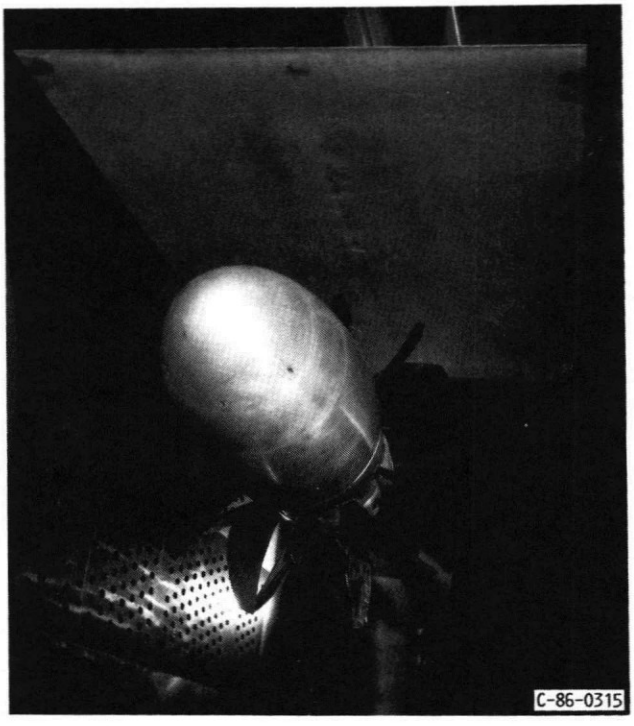

(b) PHOTOGRAPH.

FIGURE 3. - ACOUSTIC PLATE FOR NEAR FIELD NOISE MEASUREMENT IN NASA LEWIS 8 BY 6 FT WIND TUNNEL.

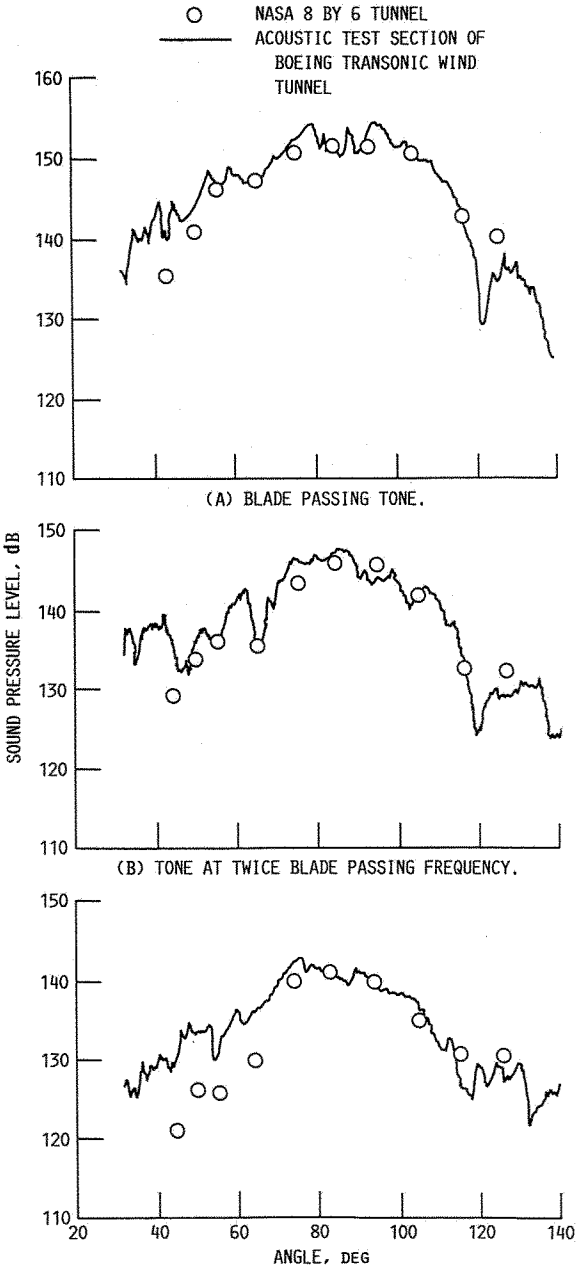

FIGURE 4. - COMPARISON OF ACOUSTIC DATA FOR THE F7/A7 COUNTERROTATION PROPELLER MODEL IN THE NASA LEWIS 8 BY 6 AND BOEING TRANSONIC WIND TUNNELS. (100% SPEED, M = 0.72, DATA ADJUSTED TO BOEING CONDITIONS ON A 67 CM (2.2 FT) SIDELINE).

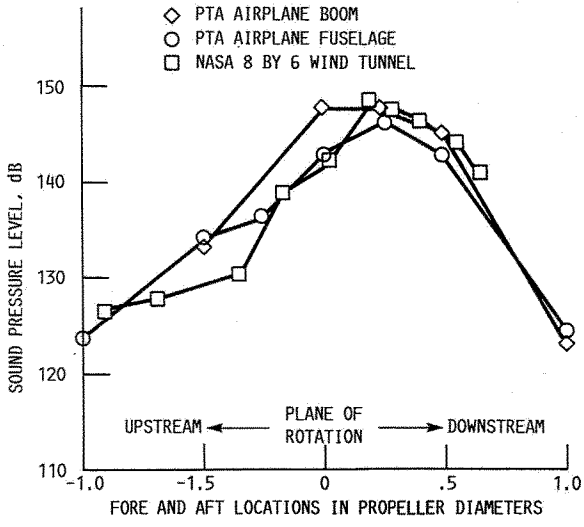

FIGURE 5. - COMPARISON OF SCALED ACOUSTIC DATA FROM THE 8 BY 6 WIND TUNNEL WITH FULL SCALE PTA FLIGHT DATA, M = 0.8 (DATA CORRECTED TO PTA FUSELAGE CONDITIONS ON A 3.05 M (10 FT) SIDELINE).

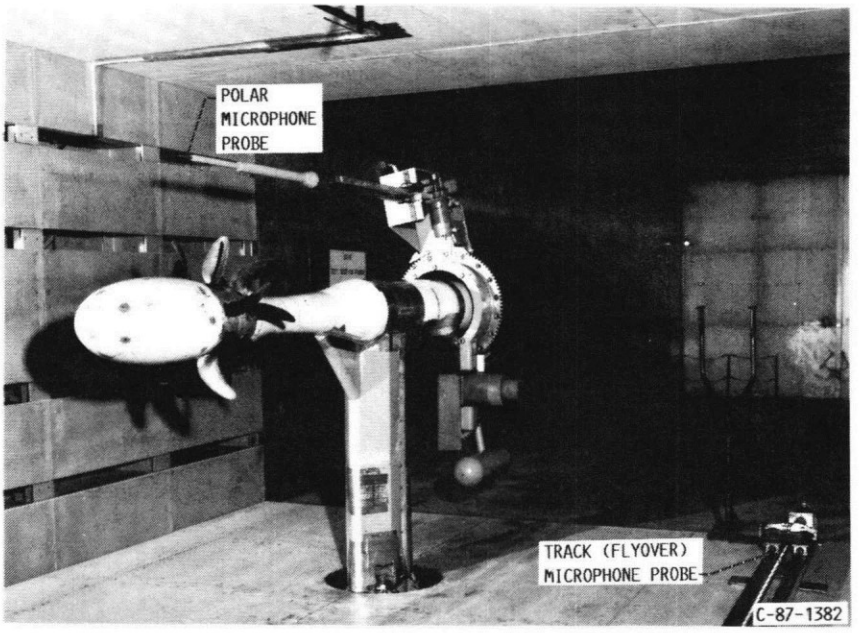

FIGURE 6. - PHOTOGRAPH OF THE UDF COUNTER-ROTATING TURBOPROP MODEL IN THE 9x15 ANECHOIC WIND TUNNEL.

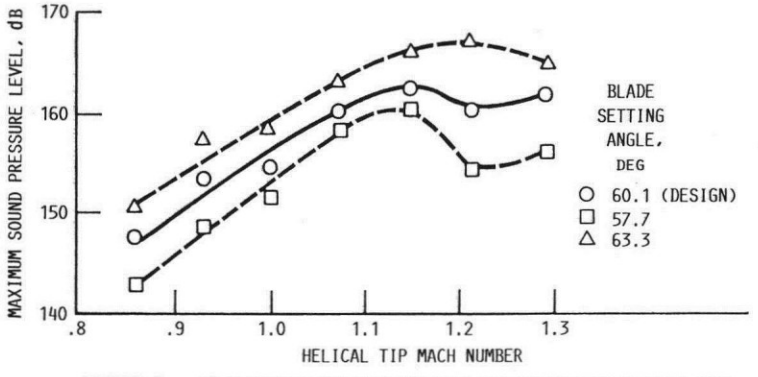

FIGURE 7. - SR-7 PEAK BLADE PASSING TONE VARIATION WITH HELICAL TIP MACH NUMBER; CONSTANT ADVANCE RATIO, 3.06.

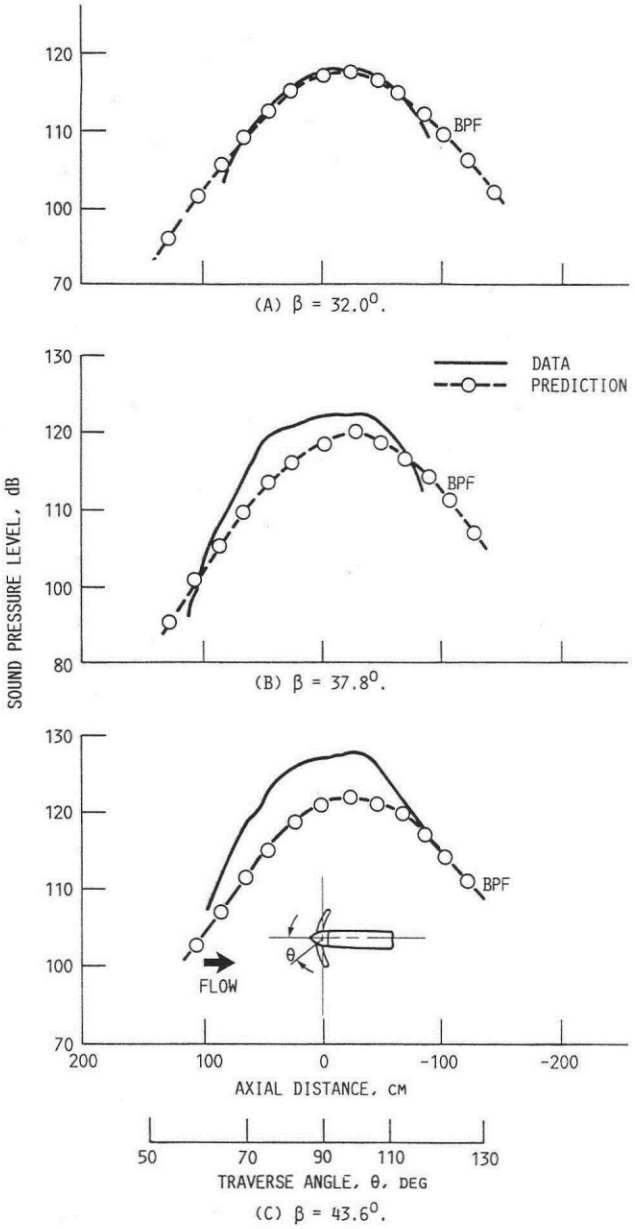

FIGURE 8. - COMPARISON OF SR-7A MODEL DATA WITH PREDICTION (1.68 M SIDELINE, J = 0.886, M_0 = 0.2).

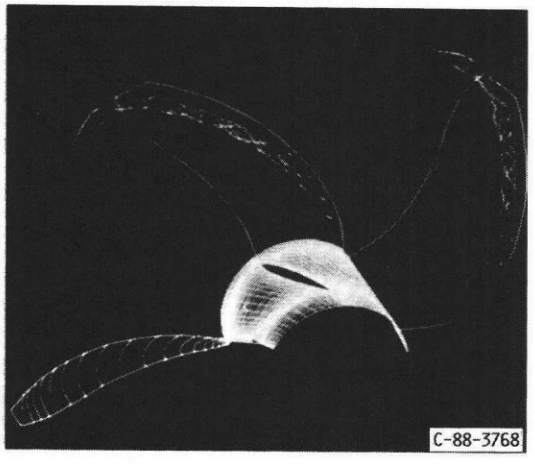

FIGURE 9. - COMPUTED PARTICLE PATHS ON AN ADVANCED PROPELLER, MACH 0.2; J = 1.0.

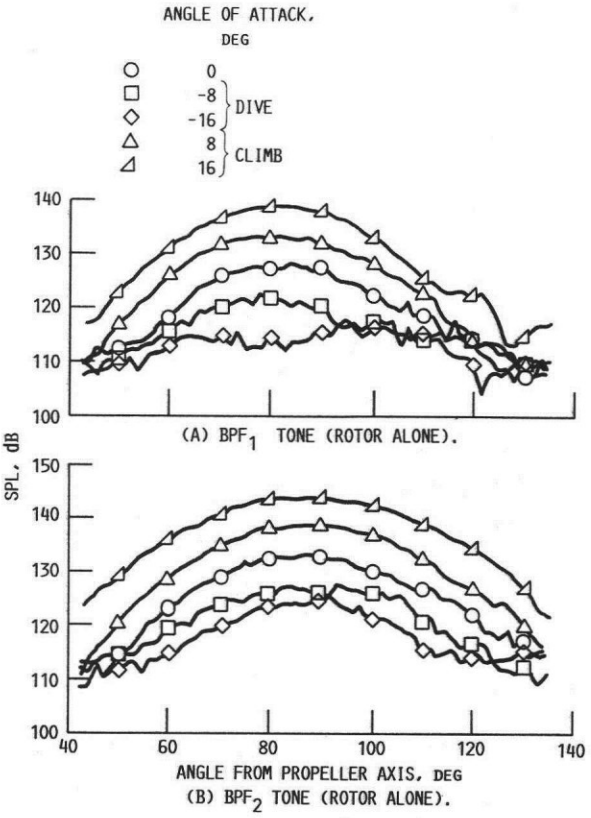

FIGURE 10. - TONE DIRECTIVITY ALONG A 61-MC(24-IN.) SIDELINE FOR SEVERAL PROPELLER AXIS ANGLES OF ATTACK. (F7/A7, 11X9, 90% SPEED M = 0.2)

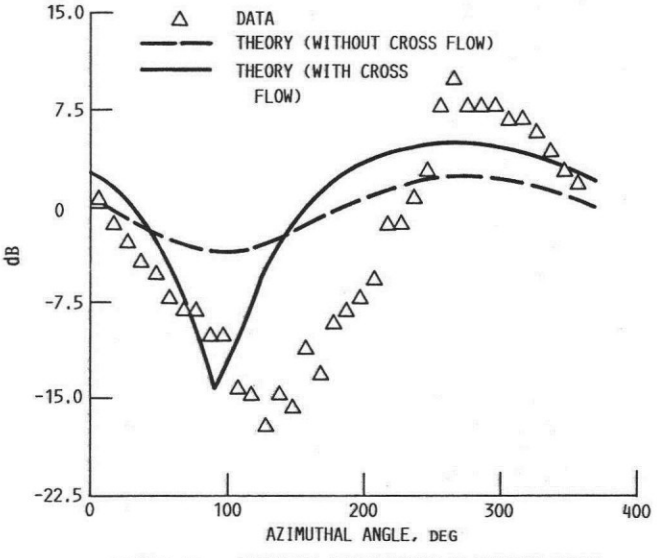

FIGURE 11. - AZIMUTHAL DIRECTIVITY OF FORWARD ROTOR FUNDAMENTAL TONE FOR PROPELLER AT ANGLE OF ATTACK, F7/A7, 11X9 PROPELLER, +16° ANGLE OF ATTACK, M = 0.2.

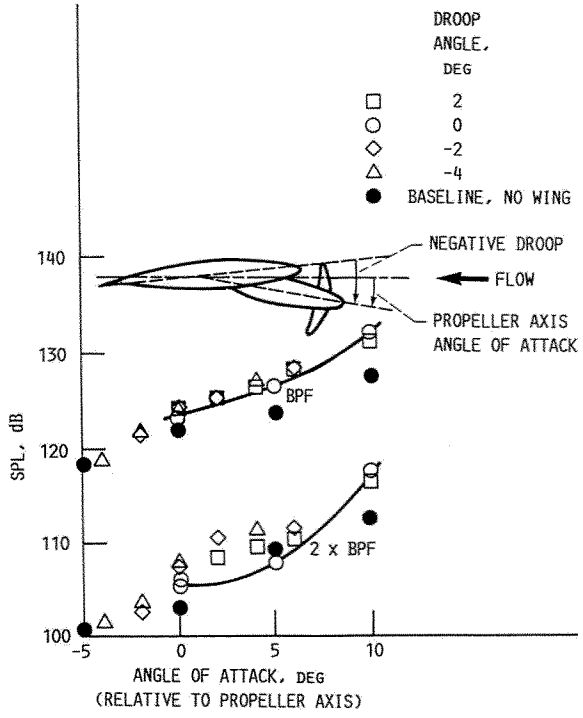

FIGURE 12. - EFFECT OF PROPELLER DROOP ON MAXIMUM TONE NOISE, STRAIGHT WING, 0.54 CHORD SPACING, U_t = 244 M/SEC (800 FT/SEC), β = 37.8°, M = 0.2.

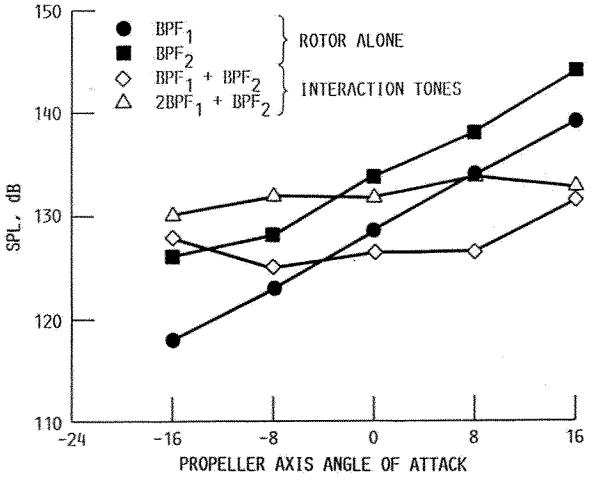

FIGURE 14. - ANGLE OF ATTACK EFFECTS ON COUNTERROTATION TONES IN AFT PROPELLER PLANE, BELOW THE AIRCRAFT. F7/A7, 11X9; β_1/β_2 = 36.4°/36.5°; 90% SPD; M_∞ = 0.2.

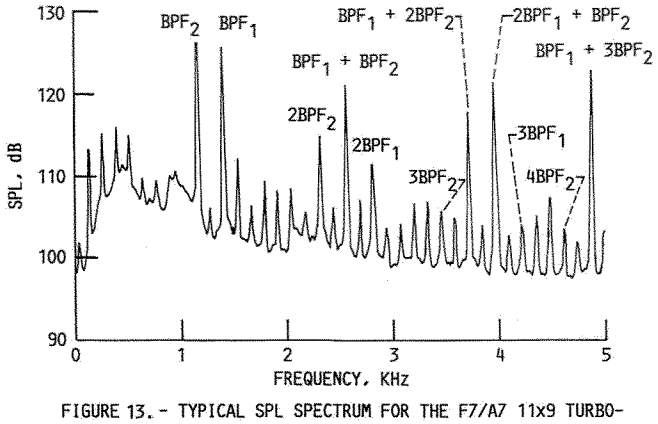

FIGURE 13. - TYPICAL SPL SPECTRUM FOR THE F7/A7 11X9 TURBOPROP. DATA IS FOR THE FIXED FLOOR MICROPHONE IN THE PROPELLER PLANE. (90 PERCENT SPD, α = 0°, β_1/β_2 = 36.4°/36.5°, NORMINAL BLADE SPACING)

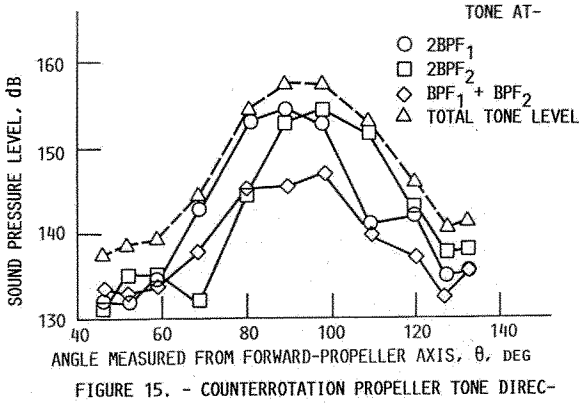

FIGURE 15. - COUNTERROTATION PROPELLER TONE DIRECTIVITY AT CRUISE CONDITIONS F1/A1, 9X8, M = 0.76, 100% SPEED.

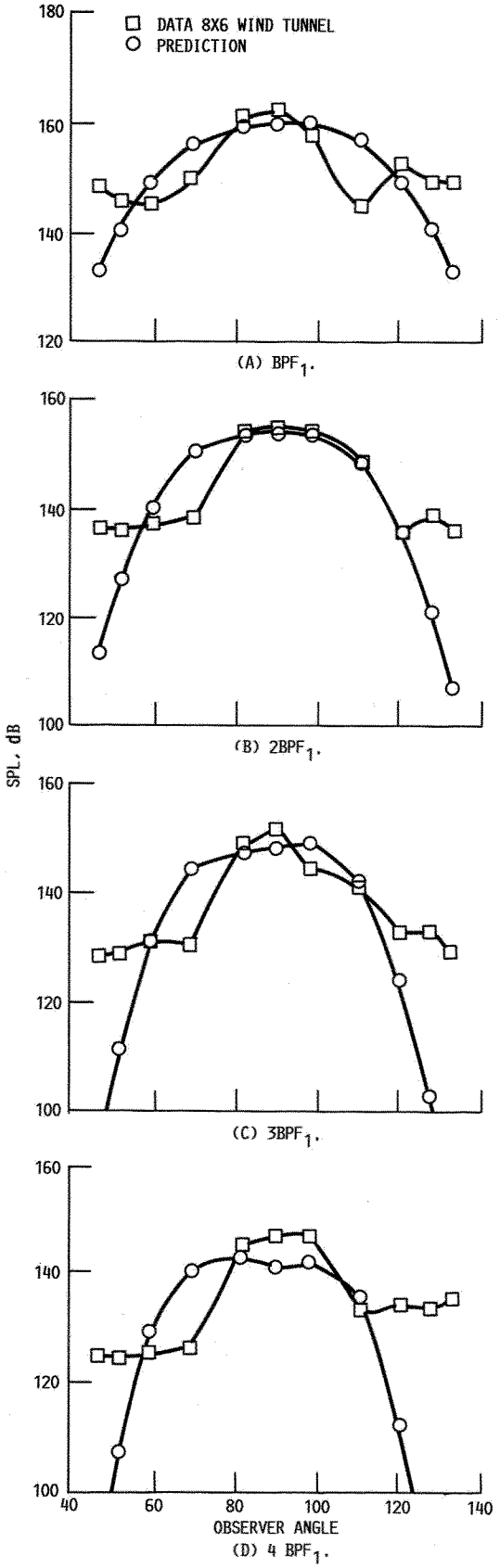

FIGURE 16. - COUNTERROTATION PROPELLER NEAR FIELD TONE DIRECTIVITY AT CRUISE CONDITIONS, F1/A1, 9X8, M = 0.72, 100% SPEED.

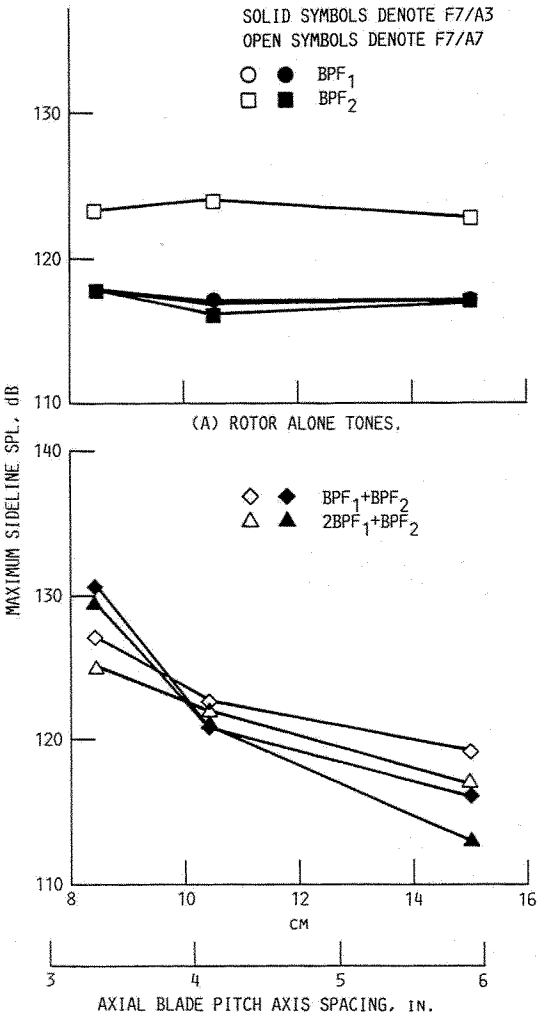

FIGURE 17. - COMPARISON OF F7/A3 AND F7/A7 BLADE ROW SPACING EFFECTS. (137-CM (54-IN.) SIDELINE, 90 PERCENT SPEED, F7/A3, β_1/β_2 = 36.4°/43.5°, F7/A7, β_1/β_2 = 36.4°/36.5°, α = 0°, M_∞ = 0.2.)

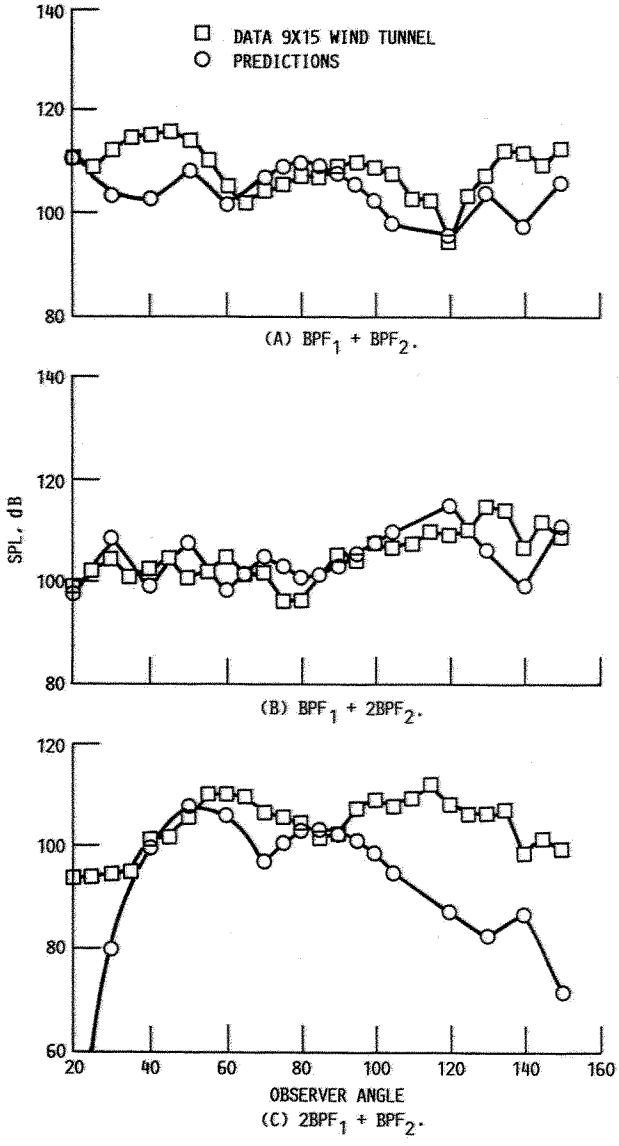

FIGURE 18. - COUNTERROTATION PROPELLER INTERACTION TONE DIRECTIVITY AT TAKEOFF/APPROACH CONDITIONS, F7/A7 11X9, M = 0.2, 80% SPEED

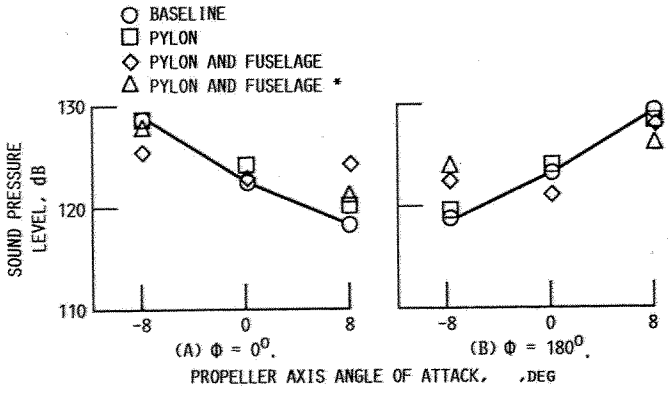

FIGURE 19. - MAXIMUM F7/A3 BPF_1 TONE LEVEL ALONG A 61-CM (24 IN.) SIDELINE AS A FUNCTION OF PROPELLER AXIS ANGLE OF ATTACK. (β_1/β_2 = 41.1°/46.4°, 80 PERCENT SPEED, M_∞ = 0.2). *BLADE SETTING ANGLES ADJUSTED FOR EQUAL TORQUE SPLIT.

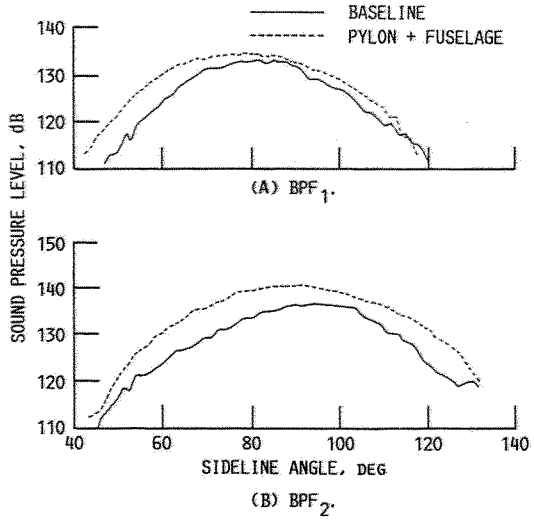

FIGURE 20. - EFFECT OF PYLON + FUSELAGE ON F7/A7 ROTOR-ALONE TONE SIDELINE DIRECTIVITY, Φ = 90°, 90% DESIGN SPEED (61 CM (24 IN.) SIDELINE, α = 0°, M_∞ = 0.2).

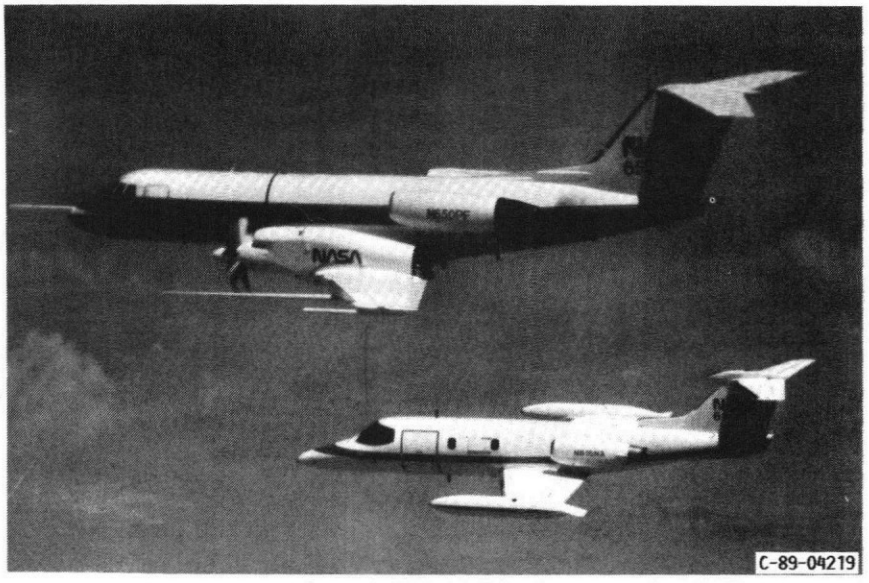

FIGURE 21. - PROPELLER TEST ASSESSMENT (PTA) GULFSTREAM II AIRCRAFT WITH 9 FOOT (2.74 M) DIAMETER SR-7L PROPELLER MOUNTED ON THE WING. LEWIS INSTRUMENTED LEARJET IN FORMATION.

FIGURE 22. - UNDUCTED FAN (UDF) ENGINE ON THE 727 AIRCRAFT.

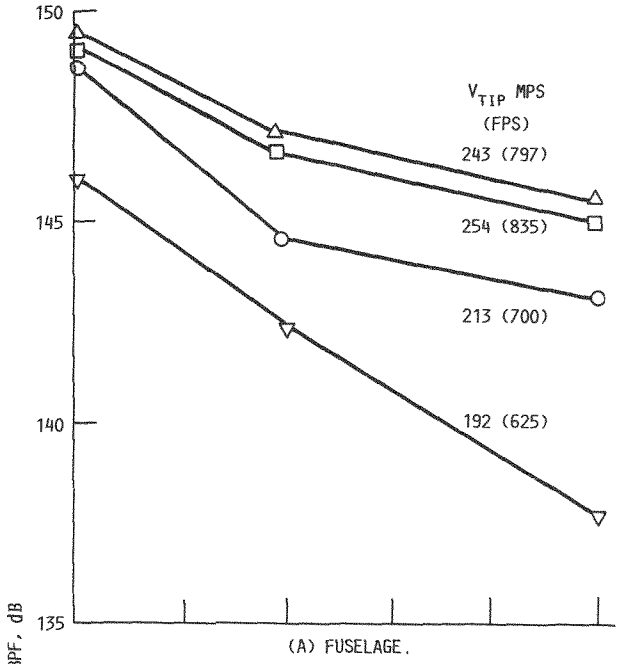

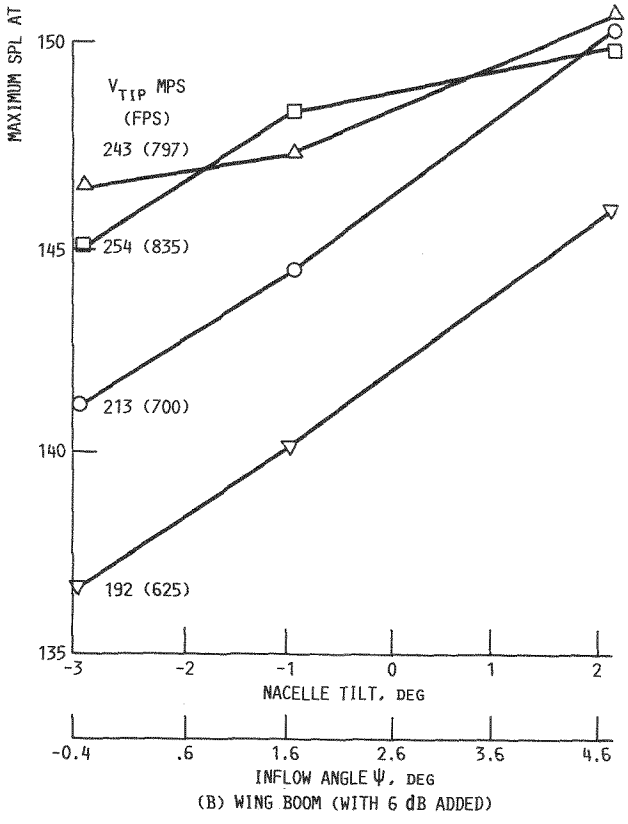

FIGURE 23. - EFFECT OF NACELLE TILT ON FUSELAGE AND WING BOOM SOUND PRESSURE LEVELS, M = 0.8, 35000 FT (10,688 M) ALTITUDE AIRCRAFT ANGLES OF ATTACK AND YAW, 1.6 AND -0.5^{0}.

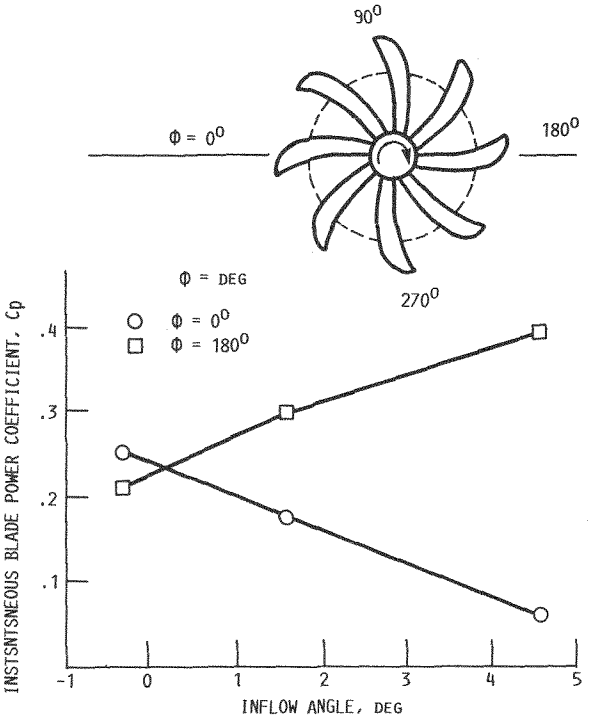

FIGURE 24. - INSTANTANEOUS BLADE POWER COEFFICIENTS FOR THE SR-7L PROPELLER ON THE PTA AIRCRAFT CALCULATED WITH A 3D UNSTEADY EULER CODE.

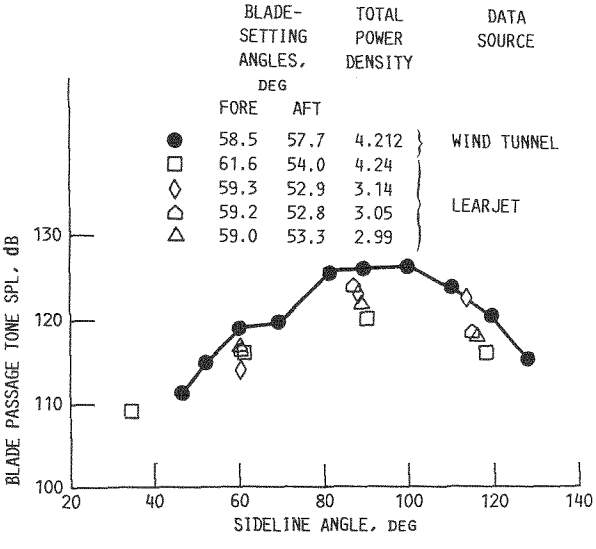

FIGURE 25. - UDF FUNDAMENTAL TONE DIRECTIVITY MEASURED IN FLIGHT, COMPARED WITH SCALED MODEL DATA: F7/A7 BLADE CONFIGURATION AT MACH 0.72 CRUISE CONDITIONS. SIDELINE DISTANCE, 47.2 M (155 FT) ALTITUDE, 10688 M (35000 FT).

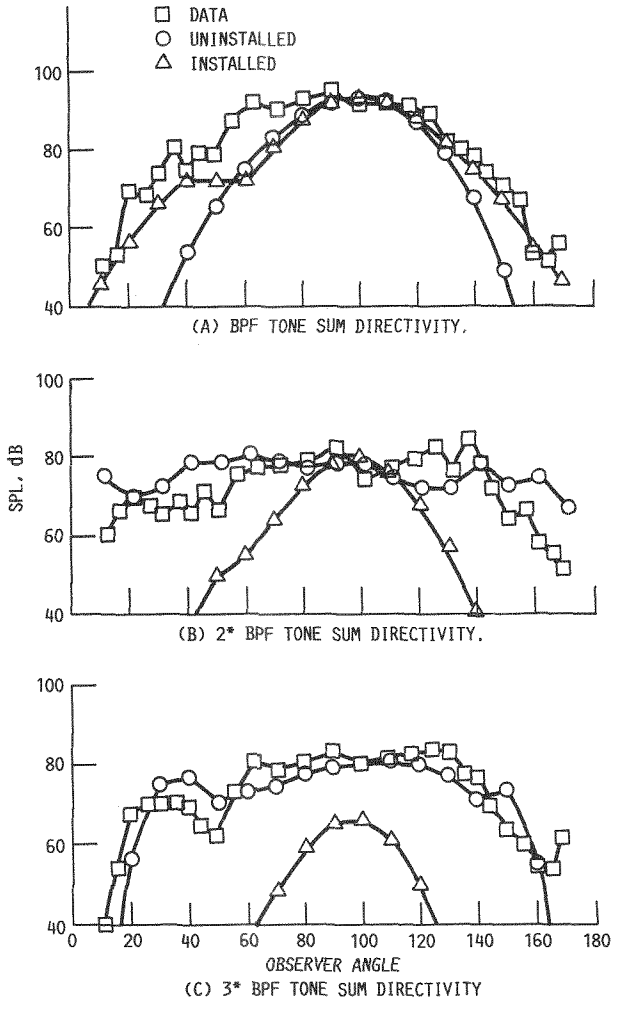

FIGURE 26. - COMPARISON OF PREDICTION WITH FLY-OVER UDF DATA FROM GROUND PLANE MICROPHONE - 100% THRUST. M = 0.255, PRESSURE ALTITUDE = 1323 M (4340 FT).

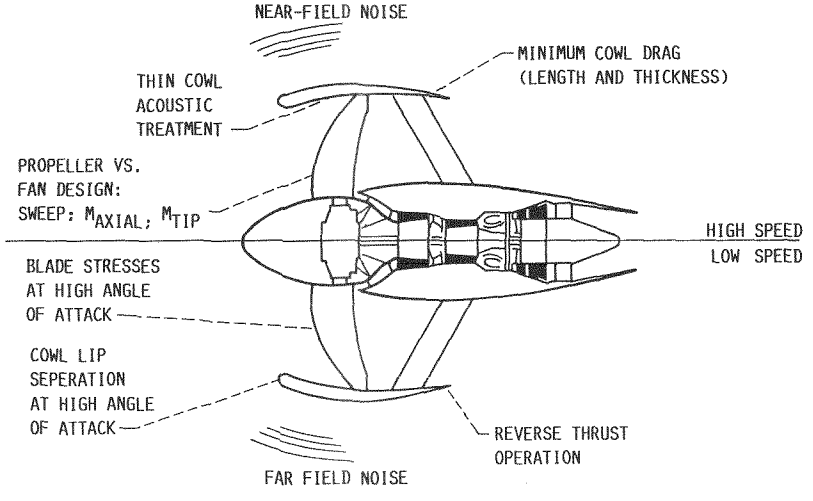

FIGURE 27. - TECHNICAL ISSUES FOR HIGH-SPEED DUCTED PROPELLERS (VERY HIGH BYPASS FANS).

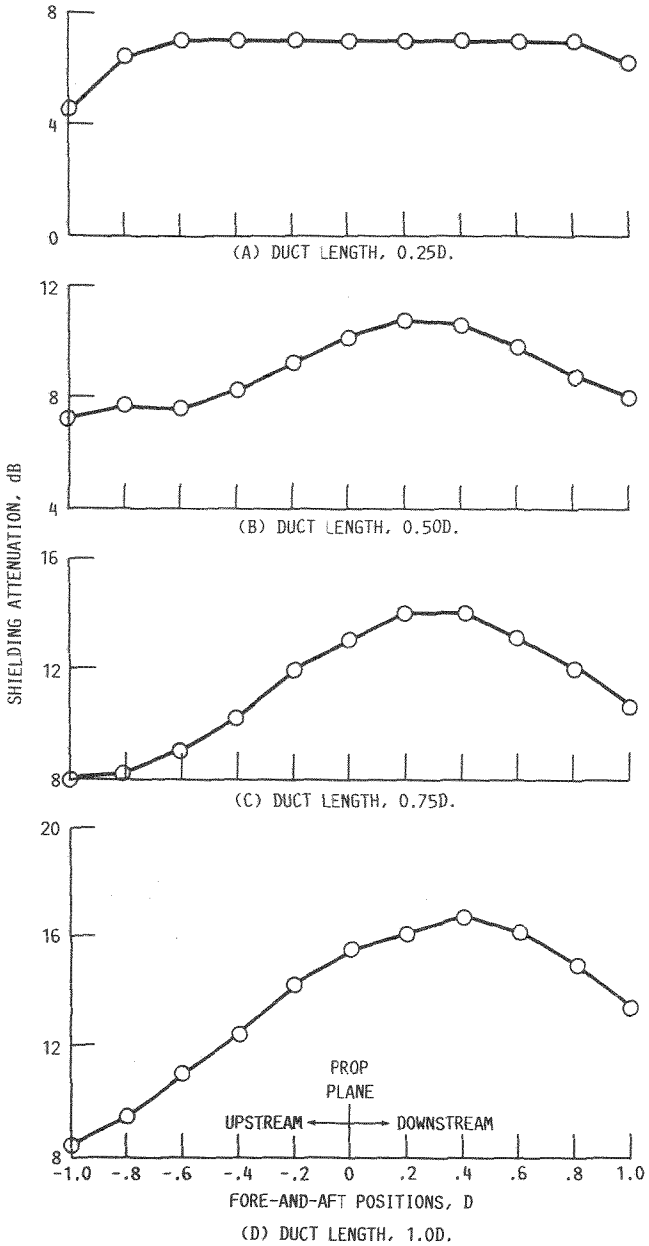

FIGURE 28. - ESTIMATED SHIELDING ATTENUATION (PROPELLER ONE-THIRD OF DUCT FROM INLET, WAVE LENGTH = D/2.

TABLE I. - PROPELLER ACOUSTIC ANALYSIS METHODS

(a) Steady regime

Aerodynamic input	Acoustic model		Single (SR) or counterrotation (CR)	Status[a]
	Type	Domain		
(A) Lifting line	Linear	Time	SR	O
(B) Lifting surface	↓	Frequency	↓	↓
(C1) Euler		Time		
(C2)		Frequency		
(C3)	Nonlinear/ Linear	Time		UD
(D) Navier-Stokes	Linear	Time	↓	UD

(b) Unsteady regime

(E1) Hybid aero/ linear lift response	Linear	Frequency	CR	O
(E2) Actuator disk/ linear lift response	↓	Frequency	SR[b]	O
(E3) Actuator disk/ linear lift response		Frequency	CR[b]	O
(F) Lifting surface		Frequency	SR[b]	O
			CR[b]	UD
(G) Euler		Time	SR	UD
			CR	UD
(H) Navier-Stokes		Time	SR	UD
	↓		CR	P

[a]Status: O-Operational UD-Underdevelopment, P-Planned.
[b]Installed.